A Novel Pd Precursor Loaded γ-Al$_2$O$_3$ with Excellent Adsorbent Performance for Ultra-Deep Adsorptive Desulfurization of Benzene

Jiyang Xie, Kelvin Ng, Yunsheng Dai, Jinke Jiang, Juan Yu, Anli Gao, Hongqin Wang, Xinyu Huang, Weiping Liu,* and Shuailong Guo*

Fabricating highly water-soluble and chlorine-free precursors from Pd complexes remains challenging. Here, a novel Pd precursor (ammonium dinitrooxalato palladium(II) ((NH$_4$)$_2$[Pd(NO$_2$)$_2$(C$_2$O$_4$)]·2H$_2$O)) is synthesized to address this challenge. Additionally, a Pd/Al$_2$O$_3$ adsorbent is prepared using γ-Al$_2$O$_3$ as a base material to host Pd. The ligand action of the Pd complex forms single Pd atoms and Pd sub-nano clusters on the surface of γ-Al$_2$O$_3$. Pd/Al$_2$O$_3$-4 as an adsorbent is evaluated using the benzene ultra-deep desulfurization procedure, wherein thiophene is used as a probe molecule. The sulfur adsorption capacity of Pd/Al$_2$O$_3$-4 is 1.76 mg g^{-1} for the ultra-deep adsorptive desulfurization of benzene at a sulfur concentration of 50 ppm. The sulfur adsorption capacity of the new Pd/Al$_2$O$_3$-4 adsorbent is 21.8% higher than that of a commercial Pd/Al$_2$O$_3$ adsorbent. In addition, the stability and durability of Pd/Al$_2$O$_3$-4 are investigated at a sulfur concentration of 1 ppm. The Pd/Al$_2$O$_3$-4 adsorbent achieves ≈100% thiophene removal after 434 h, which is 62 h more than the time required by the commercial Pd/Al$_2$O$_3$ adsorbent. The novel Pd precursor shows excellent potential for industrial applications, and the Pd/Al$_2$O$_3$-4 adsorbent can be produced on a mass scale of 500 kg per batch.

1. Introduction

In specific heterogeneous catalytic reactions, such as benzene hydrogenation and hydrodesulfurization, catalysts are particularly sensitive to sulfur compounds (such as hydrogen sulfide, thiophene, and thioether), which can poison the catalyst and render it inactive.[1–7] In the ultra-deep adsorptive desulfurization of benzene, poor desulfurization results were reported because the interaction between the traditional adsorbents and organic sulfur species was inefficient even at low concentrations, and the adsorbent did not perform as anticipated.[8,9] Therefore, the industry has switched to using palladium alumina (Pd/Al$_2$O$_3$) as an alternative adsorbent in the ultra-deep adsorptive desulfurization of benzene because of its better performance. However, Pd/Al$_2$O$_3$ has certain shortcomings, including the difficulty in the dissolution and adsorption of palladium chloride (PdCl$_2$) precursor and the complexity involved in the preparation of Pd/Al$_2$O$_3$. From an economic perspective, the price hikes in recent years have significantly compromised the large-scale application of Pd/Al$_2$O$_3$ adsorbents.[10] Therefore, the industry requires an easy adsorbent preparation technique for enhancing the reactivity and durability of the Pd/Al$_2$O$_3$ adsorbent. This may result in outstanding economic benefits to the ultra-deep adsorptive desulfurization of benzene.

PdCl$_2$ is the most widely used precursor in the preparation of Pd-based materials.[11–15] However, the presence of chlorine on the surface of the metal can block the active sites and hinder the effective adsorption of the reactants, resulting in negative effects on material behavior.[16–22] Additionally, chloride produces acidic gases (such as hydrochloride and chlorine) as byproducts during calcination or reduction, corroding the production equipment and causing air pollution. Organic Pd compounds (such as palladium(II)acetate (Pd(OAc)$_2$) and palladium diacetylacetonate (C$_{10}$H$_{16}$O$_4$Pd)) are commonly used as Pd precursors. However, they have low water solubilities,[23,24] and organic solvents harmful to the environment are required when they are used as precursors for preparing Pd-based

J. Xie, Y. Dai, J. Jiang, J. Yu, A. Gao, H. Wang, W. Liu, S. Guo
The State Key Laboratory of Advanced Technologies for Comprehensive Utilization of Platinum Metals
Kunming Institute of Precious Metals
Kunming 650106, China
E-mail: lwp@ipm.com.cn; shuailongguo@whu.edu.cn
J. Xie, X. Huang
State Key Laboratory of Physical Chemistry of Solid Surfaces
Collaborative Innovation Center of Chemistry for Energy Materials
National Engineering Laboratory for Green Chemical
Productions of Alcohols
Ethers and Esters
College of Chemistry and Chemical Engineering
Xiamen University
Xiamen 361005, China
K. Ng, S. Guo
Singapore Centre for 3D Printing
School of Mechanical and Aerospace Engineering
Nanyang Technological University
50 Nanyang Avenue, Singapore 639798, Singapore

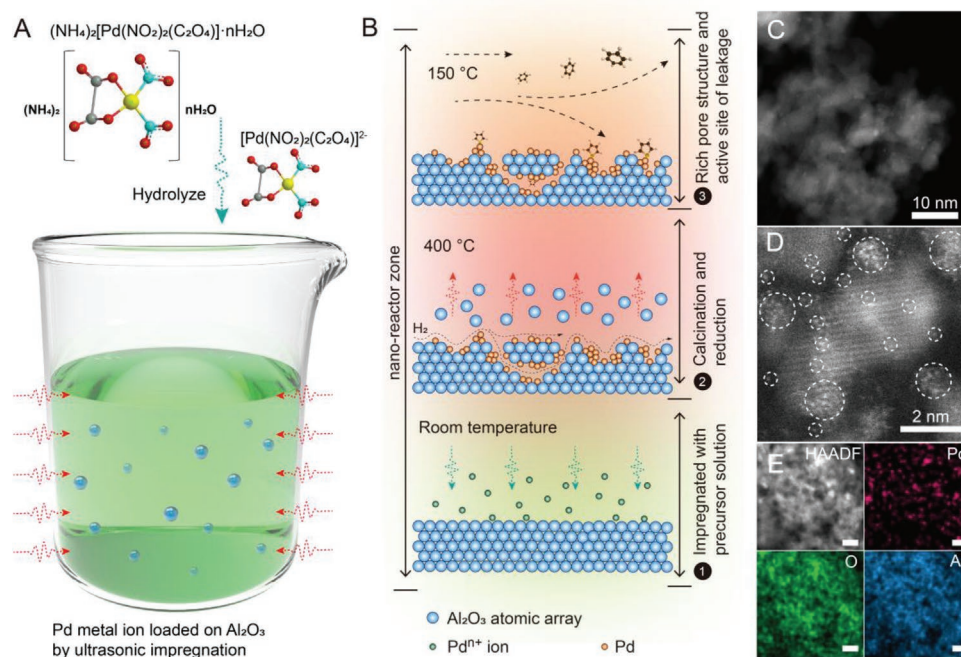The ORCID identification number(s) for the author(s) of this article can be found under https://doi.org/10.1002/adfm.202213837.

Figure 1. A,B) Schematic diagram of the preparation of the Pd/Al$_2$O$_3$-4 adsorbent. C,D) AC-STEM images of the Pd/Al$_2$O$_3$-4 adsorbent after reduction. E) HAADF image and corresponding elemental mappings of Pd, Al, and O in the Pd/Al$_2$O$_3$-4 adsorbent (scale bar is 10 nm).

materials. Thus, designing a Pd complex that is highly water-soluble, environmentally friendly, and Cl-free as a precursor is crucial for the success of Pd-based materials in desulfurization applications.

In this study, we synthesized a new Pd precursor, ammonium dinitrooxalato palladium(II) ((NH$_4$)$_2$[Pd(NO$_2$)$_2$(C$_2$O$_4$)]·nH$_2$O), and used gamma alumina (γAl$_2$O$_3$) as the base material to host the Pd adsorbent for use in the ultra-deep adsorptive desulfurization of benzene. The results are encouraging, and the new Pd precursor shows excellent potential for industrial applications. The adsorbent can be easily prepared in an environmentally friendly manner, which is also Cl free. The resulting solubility of the precursors and the strong interaction between [Pd(NO$_2$)$_2$(C$_2$O$_4$)]$^{2+}$ ions and γ-Al$_2$O$_3$ supports the creation of highly scattered Pd single atoms and sub-nanoclusters on the surface of the material. The adsorption capacity is 20% higher than that of the commercial Pd/Al$_2$O$_3$ adsorbent. This newly developed Pd-based complex has considerable potential for applications in the fields of catalysis, energy, and electronics, which are yet to be investigated.

2. Results and Discussion

The composition of the (NH$_4$)$_2$[Pd(NO$_2$)$_2$(C$_2$O$_4$)]·nH$_2$O complex, as determined via elemental analysis, is summarized in Table S1 (Supporting Information). The mass contents of Pd, carbon (C), hydrogen (H), and nitrogen (N) in (NH$_4$)$_2$[Pd(NO$_2$)$_2$(C$_2$O$_4$)]·nH$_2$O were 29.40%, 6.62%, 3.38%, and 15.40%, respectively, while the theoretical mass contents of Pd, C, H, and N in (NH$_4$)$_2$[Pd(NO$_2$)$_2$(C$_2$O$_4$)]·nH$_2$O were 29.70%, 6.70%, 3.34%, and 15.60%, respectively. The results

indicate that the actual elemental content is consistent with the theoretical content.

Figure S1 (Supporting Information) shows the Fourier-transform infrared (FT-IR) spectra of the novel Pd complex. The peak at 3435 cm^{-1} corresponds to the strong stretching vibration of water, and the peaks at 3232 and 3177 cm^{-1} correspond to the strong stretching vibration of NH$_4^+$. Additionally, the peaks at 1612 and 1401 cm^{-1} correspond to the strong asymmetric and symmetric stretching vibrations, respectively, of C$_2$O$_4^{2-}$. Moreover, the peaks at 1137 and 1311 cm^{-1} correspond to the NO$_2^-$ strong symmetric stretching vibration. Meanwhile, the peaks at 558 and 527 cm^{-1} are attributed to the weak symmetric stretching vibrations of Pd—O and Pd—N, respectively. The v_{as}-v_s value in the FT-IR spectra is higher than 200 cm^{-1}, suggesting that C$_2$O$_4^{2-}$ acts as a monodentate ligand. These results indicate that the target Pd complex contains H$_2$O, NH$_4^+$, C$_2$O$_4^{2-}$, and NO$_2^-$ functional groups and Pd—O and Pd—N coordination bonds.

A downfield shift of signals in the ^{13}C nuclear magnetic resonance (^{13}C-NMR) spectrum of the palladium complex from 174 ppm (Na$_2$C$_2$O$_4$) to 167 ppm (COO-Pd) confirms its coordination owing to Pd binding (Figure S2, Supporting Information). In an aqueous solution, the complex dissociates into NH^{4+} and the coordination anion [Pd(NO$_2$)$_2$(C$_2$O$_4$)]$^{2-}$, which can be detected using electrospray ionization–mass spectroscopy (ESI-MS) at m/e = 140 (Figure S3, Supporting Information).[25,26] The atomic weight of Pd corresponds to ^{104}Pd, a naturally stable isotope. The results show that the synthesized Pd complex had the chemical structure of (NH$_4$)$_2$[Pd(NO$_2$)$_2$(C$_2$O$_4$)]·nH$_2$O. The spatial result of a four-coordinated structure formed by the coordination of C$_2$O$_4^{2-}$ and NO$_2^-$ with Pd is shown in **Figure 1**A in light yellow (Figure S4, Supporting Information).

ADVANCED
SCIENCE NEWS
www.advancedsciencenews.com

ADVANCED
FUNCTIONAL
MATERIALS
www.afm-journal.de

The preparation of the Pd/Al$_2$O$_3$-4 adsorbent is facile, as shown in Figure 1A,B. First, $(NH_4)_2[Pd(NO_2)_2(C_2O_4)]\cdot nH_2O$ is dissolved in deionized water to obtain $[Pd(NO_2)_2(C_2O_4)]^{2-}$ cations, and subsequently the $[Pd(NO_2)_2(C_2O_4)]^{2-}$ cations are deposited on the surface of γ-Al$_2$O$_3$ via electrostatic interaction. During calcination, the NO$_2-$ and C$_2$O$_4{}^{2-}$ ions that coordinate with Pd^{2+} decompose, and the remaining Pd^{2+} is anchored on the surface of alumina because of strong interactions with γ-Al$_2$O$_3$ to form Pd—O—Al. Because the target complex has more and larger ligands than other precursors, the mutual repulsion between complexes makes Pd highly dispersed on the surface of Al$_2$O$_3$. Finally, after calcination and reduction in a H$_2$ atmosphere, some Pd single atoms and Pd sub-nano clusters co-exist on the surface of Al$_2$O$_3$. (Figure 1C,D). During adsorption, thiophene molecules in the benzene solution are adsorbed by Pd single atoms and Pd sub-nano clusters via π-complexation and S–M adsorption.[27,28] The FTIR spectra of the Pd/Al$_2$O$_3$-4 adsorbent confirm the absence of absorption bands ascribable to C$_2$O$_4{}^{2-}$ and NO$_2{}^-$ ligands after high-temperature pyrolysis (Figure S5, Supporting Information). The results of thermogravimetric analysis (TGA) indicate the detachment of coordinating ligands at $\approx$175 °C and their complete removal above 241 °C (Figure S6, Supporting Information). Based on the FTIR and TGA results, we infer that no ligand residue was present on the surface of Pd/Al$_2$O$_3$-4. Transmission electron microscopy (TEM) and high-resolution TEM (HR-TEM) images do not show the presence of Pd nanoparticles on Pd/Al$_2$O$_3$-4 (Figure S7, Supporting Information). The image of spherical aberration-corrected high-angle annular dark-field scanning transmission electron microscopy (AC-STEM) exhibits small bright dots that signify the presence of Pd sub-nano clusters (Figure 1D), and the Pd sub-nano cluster is assembled with 8–10 bright-dot atoms, enclosed in white cycles. Elemental mapping of Pd via energy-dispersive spectroscopy (EDS) shows that Pd is highly dispersed on the surface of Al$_2$O$_3$ (Figure 1E). The AC-STEM results indicate that the generated sub-nano Pd clusters have an average size of $\approx$0.91 nm (Figure S8, Supporting Information). The Pd content of Pd/Al$_2$O$_3$-4, as determined via inductively coupled plasma atomic emission spectroscopy (ICP-AES), is 0.98 wt.% (Table S2, Supporting Information). However, under the same preparation conditions, Pd nanoparticles are dispersed on the surface of γ-Al$_2$O$_3$ in the Pd/Al$_2$O$_3$ adsorbents prepared using PdCl$_2$, Pd(OAc)$_2$, and Pd(NO$_3$)$_2\cdot nH_2$O precursors. Their average particle sizes are 7.6, 3.6, and 3.6 nm, respectively (Figures S9–S11, Supporting Information). Downsizing the metal particles to sub-nano clusters is a straightforward method to increase the utilization efficiency of the metal. The resulting sub-nano clusters display good activity performance in numerous reactions. Thus, Pd/Al$_2$O$_3$-4 exhibits a higher metal dispersion, which may provide more adsorption sites to absorb thiophene molecules in a benzene solution.

Figure 2A shows the powder X-ray diffraction (PXRD) results of the prepared adsorbents. Only the typical crystal phase of γ-Al$_2$O$_3$ is detected in the Al$_2$O$_3$ support and Pd adsorbent. The peaks at $2\theta = 19.6°$, $31.9°$, $37.6°$, $39.5°$, $45.8°$, $60.5°$, and $66.8°$, may be attributed to the (1 1 1), (2 2 0), (3 1 1), (2 2 2), (4 0 0), (5 1 1), and (4 4 0) crystal planes of Al$_2$O$_3$, respectively (JCPD No. 29–0063).[29] The diffraction peaks for Pd species, which generally appear at $\approx$40.1°, 46.7°, 68.1°, 82.1°, and 86.6° (JCPD No. 05–0681), are missing. This suggests the uniformity and high dispersity of the Pd species on the support surface, which is consistent with the characterization results of AC-STEM.

The local environment of the Pd species on the Pd/Al$_2$O$_3$ adsorbents, as investigated via CO-DRIFT spectra, is shown in Figure 2B. A low-intensity peak at 2063 cm^{-1} and another peak at 1915 cm^{-1} are observed in the spectrum of Pd/Al$_2$O$_3$-1 corresponding to the bridge-adsorbed CO on small Pd clusters and threefold adsorbed CO on Pd nanoparticles, respectively.[30–32] The Pd/Al$_2$O$_3$-1 and Pd/Al$_2$O$_3$-2 adsorbents exhibit the same CO vibration frequencies. Compared with the Pd/Al$_2$O$_3$-1 adsorbent, the CO vibration frequencies of Pd/Al$_2$O$_3$-3 and Pd/Al$_2$O$_3$-4 are blue-shifted to 2072 and 1930 cm^{-1}, and 2084 and 1927 cm^{-1}, respectively. These results suggest that the electron density cloud of Pd on Pd/Al$_2$O$_3$-4 is low owing to the transfer of electrons from Pd to the Al$_2$O$_3$ support. The peak observed at 2169 cm^{-1} may be attributed to the stretching frequency of linear-adsorbed CO on the isolated Pd sites in an on-top configuration with high dispersion. This confirms the coexistence of Pd single atoms and ultra-small Pd clusters on γ-Al$_2$O$_3$, which is consistent with the AC-STEM characterization results. The results for the dispersion of Pd atoms in the Pd/Al$_2$O$_3$-4 adsorbent, as determined via CO titration, are close to 72%, which is
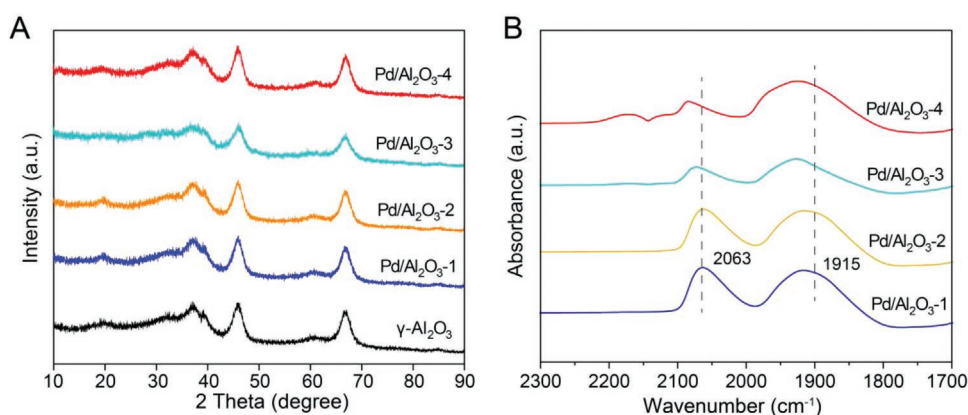

Figure 2. A) The PXRD patterns of the Al$_2$O$_3$ and Pd/Al$_2$O$_3$ adsorbents and B) CO-DRIFT spectra of the Pd/Al$_2$O$_3$ adsorbents.

**ADVANCED
SCIENCE NEWS**

www.advancedsciencenews.com

**ADVANCED
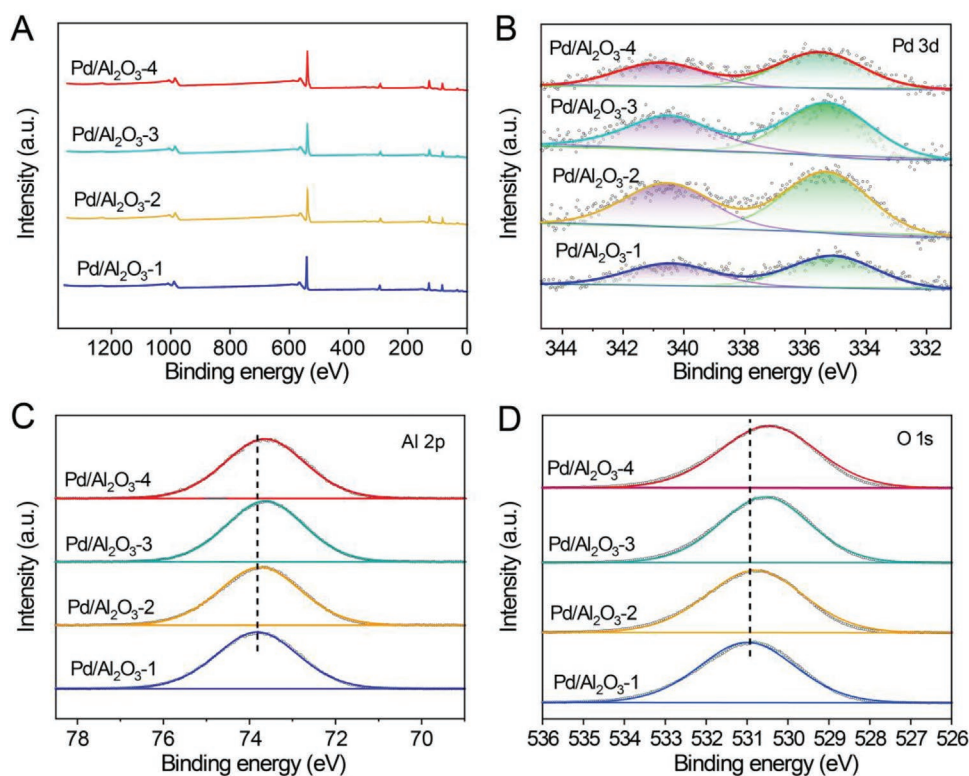FUNCTIONAL
MATERIALS**

www.afm-journal.de

Figure 3. A) Spectra and curves of the Pd/Al$_2$O$_3$ adsorbents. XPS spectra of B) Pd 3d, C) Al 2p, and D) O 1s in the Pd/Al$_2$O$_3$ adsorbents.

higher than those of other three Pd/Al$_2$O$_3$ adsorbents (Table S2, Supporting Information).

The compositions and chemical environments of the Pd/Al$_2$O$_3$ adsorbent surfaces were investigated via X-ray photoelectron spectroscopy (XPS). The spectra and curves obtained by deconvolution simulation are shown in **Figure 3**A. Figure S12 (Supporting Information) shows that the Al 2p and O 1s binding energies in the Al$_2$O$_3$ support are 73.93 and 531.01 eV, respectively. Similarly, the binding energies for Al 2p and O 1s in the Pd adsorbents exhibit values ranging from 73.81 and 530.95 eV for Pd/Al$_2$O$_3$-1, 73.72 and 530.71 eV for Pd/Al$_2$O$_3$-2, 73.58 and 530.52 eV for Pd/Al$_2$O$_3$-3, and 73.50 and 530.41 eV for Pd/Al$_2$O$_3$-4. The binding energies of Al 2p and O 1s in the Pd/Al$_2$O$_3$ adsorbents are shifted to a lower value than that of the Al$_2$O$_3$ support, implying that the interaction between the Al$_2$O$_3$ support and Pd causes electron transfer from the Pd to the Al$_2$O$_3$ support. After careful deconvolution of the Pd 3d peaks, the peaks located at binding energies of 335.07 and 340.33 eV are assigned to Pd 3d$_{5/2}$ and Pd 3d$_{3/2}$ of Pd on the Pd/Al$_2$O$_3$-1 adsorbent, respectively. Compared with the Pd/Al$_2$O$_3$-1 adsorbent, the Pd binding energies of the other three Pd/Al$_2$O$_3$ adsorbents are shifted to higher values. The Pd binding energy is different for each of the control samples, namely, 340.47 and 335.21 eV for Pd/Al$_2$O$_3$-2, 340.68 and 335.42 eV for Pd/Al$_2$O$_3$-3, while Pd/Al$_2$O$_3$-4 has recorded values of 341.03 and 335.77 eV.[33,34] The XPS results indicate that the interaction between the support and Pd species, formed by loading various Pd precursors on the same Al$_2$O$_3$ support surface after calcination and reduction, is different because of the effect of ligands. Furthermore, it also suggests that the interaction between Pd

in the (NH$_4$)$_2$[Pd(NO$_2$)$_2$(C$_2$O$_4$)]·nH$_2$O precursor and Al$_2$O$_3$ support after the same procedure is stronger than that in the other three precursors.

Ultra-deep desulfurization is closely related to the specific surface area and pore size of an adsorbent. The textural characteristics of the Al$_2$O$_3$ support (Figure S13, Supporting Information) and 1 wt.% Pd/Al$_2$O$_3$ adsorbent, as investigated using N$_2$ adsorption–desorption measurements, and the corresponding nitrogen adsorption–desorption isotherms and pore-size distribution curves of the samples are shown in **Figure 4**A,B. Figure 4A shows that the Pd/Al$_2$O$_3$-1 and Pd/Al$_2$O$_3$-3 samples exhibit type IV adsorption isotherms with obvious H2 hysteresis loops in the relative pressure (P/P$_0$) range of 0.6–1.0. The Pd/Al$_2$O$_3$-2 and Pd/Al$_2$O$_3$-4 samples exhibit type IV adsorption isotherms with obvious H3 hysteresis loops in the P/P$_0$ range of 0.7–1.0. These hysteresis loops may be attributed to the decomposition of ligands (such as CH$_3$OO$^-$, C$_2$O$_4^{2-}$, and NO$_2^-$), which changes the textural characteristics of the Al$_2$O$_3$ support.[35,36] Nitrogen adsorption–desorption results show that the Al$_2$O$_3$ support has a Brunauer–Emmett–Teller (BET) surface area of 270.8 m^2 g^{-1} and an average pore size of ≈10.5 nm. When Pd nanoparticles are deposited on the Al$_2$O$_3$ support surface, the BET surface area of the Pd/Al$_2$O$_3$ adsorbents are lower than that of the Al$_2$O$_3$ support (Table S2, Supporting Information). The specific surface areas of the Pd/Al$_2$O$_3$-1 and Pd/Al$_2$O$_3$-3 adsorbents are slightly different from that of the Al$_2$O$_3$ support. In contrast, the specific surface areas of the Pd/Al$_2$O$_3$-2 and Pd/Al$_2$O$_3$-4 adsorbents decrease to 236.7 and 228.2 m^2 g^{-1}, respectively. However, the pore volumes and average pore diameters of the Pd/Al$_2$O$_3$-2 and Pd/Al$_2$O$_3$-4 adsorbents

**ADVANCED
SCIENCE NEWS**

www.advancedsciencenews.com

**ADVANCED
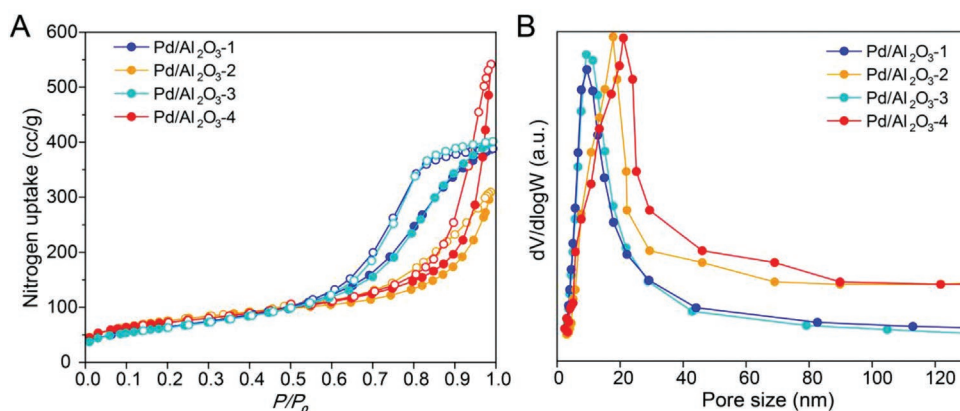FUNCTIONAL
MATERIALS**

www.afm-journal.de

Figure 4. A) Nitrogen absorption isotherms and B) pore-size distributions of the Pd/Al$_2$O$_3$ adsorbents.

increase to 0.62 cm^3 g^{-1} and 18.7 nm and 0.67 cm^3 g^{-1} and 21.3 nm, respectively. In the adsorptive desulfurization process, a large pore volume in the adsorbent can prevent the "micropore filling effect" and expose more active sites.[37] In addition, larger mesopores allow bulkier thiophenes to reach the active adsorption sites, and they are beneficial for mass transport, making mesopores favorable for the capture of adsorbates. However, these results suggest that significant variation in the adsorption capacity among Pd/Al$_2$O$_3$-1, Pd/Al$_2$O$_3$-2, Pd/Al$_2$O$_3$-3, and Pd/Al$_2$O$_3$-4 adsorbents cannot be solely attributed to a slight difference in surface area.

The sulfur adsorption capacities of Pd/Al$_2$O$_3$-1, Pd/Al$_2$O$_3$-2, Pd/Al$_2$O$_3$-3, and Pd/Al$_2$O$_3$-4 after 12 h of ultra-deep benzene adsorptive desulfurization at 120 °C are 0.96, 0.97, 1.04, and 1.18 mg g^{-1}, respectively, indicating a higher activity of the Pd/Al$_2$O$_3$-4 adsorbent than that of Pd/Al$_2$O$_3$ (**Figure 5**A). This may be attributed to the smaller particle size of sub-nano clusters and better dispersion of Pd on the surface of the Pd/Al$_2$O$_3$-4 adsorbent, which allows the Pd/Al$_2$O$_3$-4 adsorbent to provide more adsorption sites compared to other Pd/Al$_2$O$_3$ adsorbents. Additionally, when the adsorption temperature is increased to 150 °C, the sulfur adsorption capacities of
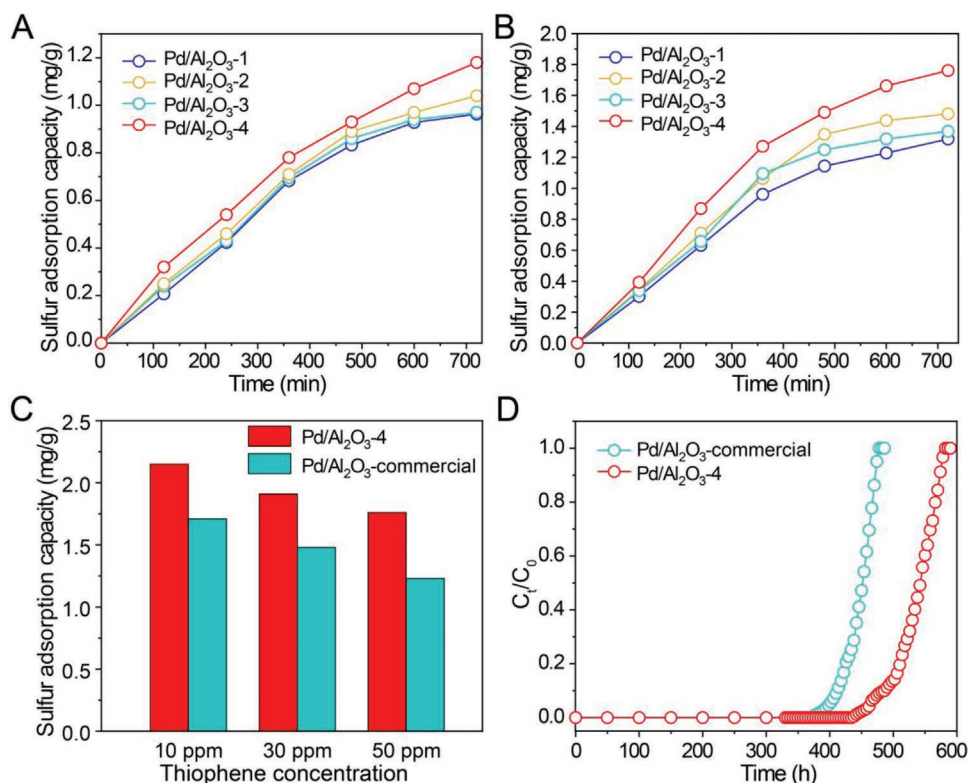

Figure 5. A) Sulfur adsorption capacity of various adsorbents at 120 °C. B) Sulfur adsorption capacity of various adsorbents at 150 °C. C) Sulfur adsorption capacities of the Pd/Al$_2$O$_3$-4 and Pd/Al$_2$O$_3$-commercial adsorbents with varying thiophene concentrations. D) The durabilities of the Pd/Al$_2$O$_3$-4 and Pd/Al$_2$O$_3$-commercial adsorbents at a thiophene concentration of 1 ppm.

Pd/Al$_2$O$_3$-1, Pd/Al$_2$O$_3$-2, Pd/Al$_2$O$_3$-3, and Pd/Al$_2$O$_3$-4 are 1.32, 1.37, 1.48 and 1.76 mg g^{-1}, respectively (Figure 5B). Notably, the sulfur adsorption capacity of the three adsorbents increases with temperature because the adsorption reaction is endothermic, and a high temperature favors thiophene adsorption at the adsorption site. Compared with the Pd/Al$_2$O$_3$-4 adsorbent, thiophene is not eliminated by the Al$_2$O$_3$ support and Pd/Al$_2$O$_3$-4-U adsorbent (without hydrogen reduction) even after 12 h of adsorption (Figure S14, Supporting Information). The activities and durabilities of adsorbents are crucial elements in industrial applications. The sulfur adsorption capacities of Pd/Al$_2$O$_3$-4 and Pd/Al$_2$O$_3$-commercial after 12 h of ultra-deep benzene desulfurization with thiophene at 150 °C and at a thiophene concentration of 10 ppm are 2.18 and 1.67 mg g^{-1}, respectively. At a thiophene concentration of 30 ppm, the sulfur adsorption capacities of Pd/Al$_2$O$_3$-4 and Pd/Al$_2$O$_3$-commercial are 1.81 and 1.47 mg g^{-1}, respectively. Additionally, at a thiophene concentration of 50 ppm, the sulfur adsorption capacities of Pd/Al$_2$O$_3$-4 and Pd/Al$_2$O$_3$-commercial are 1.76 and 1.27 mg g^{-1}, respectively (Figure 5C). The results indicate that the sulfur adsorption capacity of the Pd/Al$_2$O$_3$-4 adsorbent is 38.5% higher than that of Pd/Al$_2$O$_3$-commercial at a thiophene concentration of 50 ppm. The durability of Pd/Al$_2$O$_3$-4 and Pd/Al$_2$O$_3$-commercial adsorbents was studied using ultra-deep benzene desulfurization with 1 ppm concentration of thiophene. The Pd/Al$_2$O$_3$-4 adsorbent exhibits nearly 100% of thiophene elimination at 434 h, and after 579 h, it becomes inactive. For the Pd/Al$_2$O$_3$-commercial adsorbent, tested under the same conditions, 100% thiophene elimination occurs at 372 h, and the inactivation time is 475 h. This result suggests that the durability of the Pd/Al$_2$O$_3$-4 adsorbent is 21.8% higher than that of Pd/Al$_2$O$_3$-commercial (Figure 5D). Other d-block metals (e.g., Ag, Ni, Mo, Zn, and Cu) used in fuel desulfurization were tested and compared under similar conditions, and the results are summarized in Table S3 (Supporting Information). The results indicate that the performance of other d-block metals loaded on Al$_2$O$_3$ is inferior to that of Pd/Al$_2$O$_3$-4.

The novel Pd/Al$_2$O$_3$-4 adsorbent has superior performance, such as excellent chemical activity and long-term stability. It also has various advantages, including simpler preparation methods, environment-friendliness, and cost-effectiveness. We can mass-produce ≈500 kg of the product using a simple setup (**Figure 6**). The raw material and energy consumption data for 500 kg of large-scale synthesis are listed in Table S4 (Supporting Information). The test results indicate that the Pd/Al$_2$O$_3$-4 adsorbent has excellent potential in the ultra-deep desulfurization of benzene in the industry owing to its high sulfur adsorption capacity.

3. Conclusion

In summary, a Pd/Al$_2$O$_3$-4 adsorbent was prepared using a novel (NH$_4$)$_2$[Pd(NO$_2$)$_2$(C$_2$O$_4$)]·nH$_2$O complex as the precursor, and its sulfur adsorption capacity was tested via a benzene ultra-deep adsorptive desulfurization process. The desulfurization efficiency of the Pd/Al$_2$O$_3$-4 adsorbent is nearly 100%, even at a thiophene concentration of as low as 1 ppm. Compared with the commercial Pd/Al$_2$O$_3$ adsorbent, the new Pd/Al$_2$O$_3$-4 adsorbent shows excellent stability and a 21.8% higher adsorption activity owing to the strong interaction between Pd in the (NH$_4$)$_2$[Pd(NO$_2$)$_2$(C$_2$O$_4$)]·nH$_2$O precursor and Al$_2$O$_3$ support after calcination and reduction. The resulting Pd single atoms and sub-nano clusters are highly dispersed on the surface of the Al$_2$O$_3$ support, exposing more adsorption sites. Furthermore, the adsorbent can be mass-produced in a quantity of 500 kg,
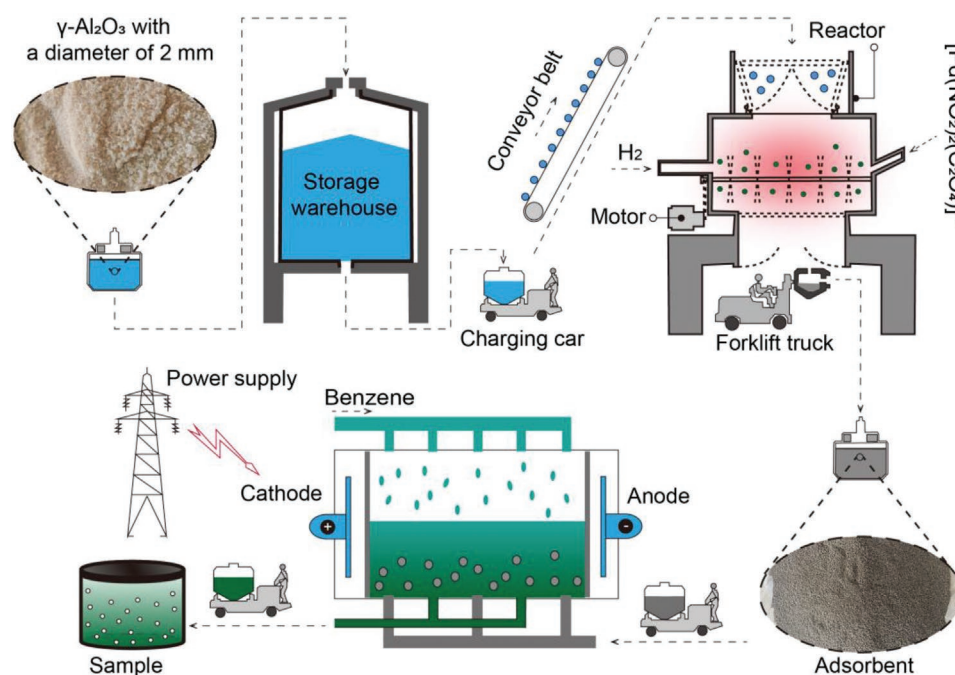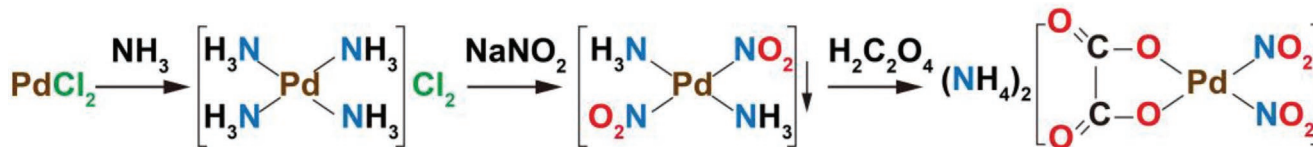

Figure 6. Flow chart of the large-scale production of 500 kg of the adsorbent.

Scheme 1. Schematic illustrations of $(NH_4)_2[Pd(NO_2)_2(C_2O_4)]\cdot nH_2O$ synthesis.

demonstrating its excellent application potential for ultra-deep desulfurization of benzene in industrial applications.

4. Experimental Section

Chemicals: Palladium chloride ($PdCl_2$, Sinopharm Chemical Reagent Co., Ltd.), palladium acetate ($Pd(OAc)_2$, Sinopharm Chemical Reagent Co., Ltd.), palladium nitrate ($Pd(NO_3)_2\cdot nH_2O$, Sinopharm Chemical Reagent Co., Ltd.), sodium nitrite ($NaNO_2$, Shanghai Chemical Reagent), aqueous ammonia (30 wt.%, Shanghai Chemical Reagent), oxalic acid dihydrate ($H_2C_2O_4\cdot2H_2O$, Sinopharm Chemical Reagent Co., Ltd.), γ-Al_2O_3 (Shandong Nanshan Aluminum Co., Ltd., China), benzene (C_6H_6, Sinopharm Chemical Reagent Co., Ltd.), acetone (C_3H_6O, Shanghai Chemical Reagent), thiophene (C_4H_4S, Sinopharm Chemical Reagent Co., Ltd.), and deionized water from a Milli-Q integral water purification system (Millipore, 18.2 $M\Omega$ cm^{-1}). All the chemicals were used without further purification.

Material Preparation: $(NH_4)_2[Pd(NO_2)_2(C_2O_4)]\cdot nH_2O$ precursor synthesis. First, 10 g of $PdCl_2$ was added to 20 mL of deionized water, followed by heating to 60 °C. Subsequently, 16.5 mL of an aqueous ammonia solution (30 wt.%) was added dropwise until $PdCl_2$ was fully dissolved. The solution was evaporated at 60 °C to obtain $[Pd(NH_3)_4]Cl_2$ powder, which was subsequently dissolved in 20 mL of deionized water and heated to 60 °C. Subsequently, 20 mL of aqueous $NaNO_2$ solution (11.28 mol L^{-1}) was slowly added to the $[Pd(NH_3)_4]Cl_2$ solution until an adequate amount of trans-$[Pd(NH_3)_2(NO_2)_2]$ pale yellow precipitate had been obtained. The pale yellow precipitate was filtered, rinsed five times with ethanol, and finally dried to obtain the trans-$[Pd(NH_3)_2(NO_2)_2]$ powder. In deionized water (400 mL), 0.52 mol of $H_2C_2O_4\cdot2H_2O$ was dissolved at 55 °C, and 12.2 g of the obtained trans-$[Pd(NH_3)_2(NO_2)_2]$ solid was added to the previously prepared reaction mixture and stirred at 100 r min^{-1} for 1 h. The solution was subsequently cooled to room temperature and filtered. Finally, the mother liquor was freeze-dried to obtain a yellow $(NH_4)_2[Pd(NO_2)_2(C_2O_4)]\cdot nH_2O$ powder. A schematic of this synthesis is shown in **Scheme 1**.

Preparation of Pd/Al$_2$O$_3$ Adsorbents: The Pd/Al_2O_3 adsorbent was prepared using an ultrasonic-assisted impregnation method. First, a certain amount of $(NH_4)_2[Pd(NO_2)_2(C_2O_4)]\cdot nH_2O$ was dissolved in 10 mL of deionized water to form $[Pd(NO_2)_2(C_2O_4)]^{2+}$ and subsequently, 7 g of γ-Al_2O_3, with a diameter of 2 mm, was immersed in the aqueous solution. The solution was then subjected to ultrasonic treatment at room temperature for 1 h, and the solid was recovered via filtration and dried in air at 120 °C for 2 h. Subsequently, the solid was calcined in a muffle furnace for 4 h at 400 °C at a ramp rate of 2 °C min^{-1}. Following heat treatment, the adsorbent was marked as Pd/Al_2O_3-4 after being reduced by H_2 gas infused at a flow rate of 25 mL min^{-1} for 4 h at 150 °C. Theoretical Pd content in Pd/Al_2O_3-4 was 1 wt.%. For comparison, palladium chloride ($PdCl_2$), palladium acetate ($Pd(OAc)_2$), and palladium nitrate ($Pd(NO_3)_2\cdot nH_2O$) precursors were used as control samples. These control samples underwent a process similar to that of Pd/Al_2O_3-4, except the solvent used. $PdCl_2$ was dissolved in 10 mL deionized water containing 1 mL of HCl (5 mol L^{-1}), $Pd(OAc)_2$ was dissolved in 10 mL of acetone, and $Pd(NO_3)_2\cdot nH_2O$ was dissolved in 10 mL of deionized water. The obtained adsorbents were denoted as Pd/Al_2O_3-1, Pd/Al_2O_3-2, and Pd/Al_2O_3-3, respectively. The theoretical Pd contents of Pd/Al_2O_3-1, Pd/Al_2O_3-2, Pd/Al_2O_3-3, and Pd/Al_2O_3-4 were

1.0 wt.% each. The actual experimental contents were determined using ICP-AES (Table S2, Supporting Information).

Adsorption Experiments: Adsorption experiments were performed on the Pd/Al_2O_3 adsorbents. The sulfur adsorption capacity of the Pd/Al_2O_3 adsorbents was tested in a fixed-bed reactor. During the experimental process, 7 g of the Pd/Al_2O_3 adsorbent was filled in the constant temperature zone of the reaction tube, and the air in the tube was removed using nitrogen. The model benzene was pumped into the preheater at a constant flow rate of 0.4 mL min^{-1} and preheated to 150 °C before being flowed into the adsorbent reaction bed. At 150 °C, the model benzene passed through the adsorbent bed at a flow rate of 0.4 mL min^{-1}. During the ultra-deep desulfurization test, the effluent liquid was collected and analyzed using a Shimadzu GC-2010 Plus equipped with a flame photometric detector. In the ultra-deep desulfurization experiment, thiophene (C_4H_4S) was used as a probe to evaluate adsorptive desulfurization. The sulfur adsorption capacity and durability of the Pd/Al_2O_3 adsorbent were tested using model benzene with a thiophene concentration of 50 and 1 ppm, respectively. The sulfur adsorption capacity was determined using Equation (1) as follows:

$$q = \frac{v}{1000m}\int_0^t (C_0 - C_t)dt \tag{1}$$

where q represents the sulfur adsorption capacity of the adsorbent (mg g^{-1}), v represents the feed volumetric flow rate (mL min^{-1}) at time t (min), and m represents the weight of the adsorbent (g).

Durability is the period when the solution passes through the adsorbent bed and the adsorbent completely absorbs thiophene. The durability of the adsorbent was estimated using Equation (2) as follows:

$$x = \frac{C_t}{C_0} \tag{2}$$

where C_t represents the product thiophene concentration at a specific time, and C_0 represents the feedstock thiophene concentration. A value of $X = C_t/C_0$ of 0 indicates complete thiophene absorption. In contrast, a value of $X = C_t/C_0$ greater than 0 but less than 1 indicates that the deactivation of the adsorbent has begun and thiophene absorption is incomplete. Additionally, a value of $X = C_t/C_0$ equal to 1 indicates that the adsorbent is deactivated completely.

Material Characterization: Low-temperature N_2 adsorption/desorption. The textural properties of the adsorbents were measured via N_2 adsorption–desorption at −196 °C using a Micromeritics Tristar II analyzer. Before the analysis, 200 mg of the samples were placed in a quartz tube and degassed at 300 °C under vacuum for 3 h. The specific surface areas of the samples were calculated using the Brunauer–Emmett–Teller method. The pore volume and size were obtained from the branches of the isotherms using the Barrett–Joyner–Halenda method. Composition analysis of the new Pd precursor. Composition analysis for C, H, and N was performed using a Carlo–Ebra instrument, whereas the Pd content was determined using the conventional hydrogen reduction gravimetric method. The chemical composition and structure of the synthesized Pd complex were characterized using FT-IR, ESI-MS, and ^{13}C NMR spectroscopies. FT-IR spectra were measured in KBr pellets using a Perkin Elmer 880 spectrometer in the range 4000–1000 cm^{-1} with a resolution of 2 cm^{-1}.

ESI-MS studies were conducted on a QTOF Premier or Quattro LC instrument equipped with an orthogonal Z-spray-electrospray interface. A capillary voltage of 3.5 kV was used in the positive ESI(+) scan mode, and the cone voltage was adjusted to a low value (typically $U_c = 5–15$ V) to control the extent of fragmentation in the source region. ^{13}C NMR spectra were recorded in D_2O on a Bruker DRX-500 MHz spectrometer relative to tetramethylsilane as an external standard. AC-STEM was performed using a JEOL ARM200 F microscope equipped with a probe-forming spherical aberration corrector. The semi-convergence angle was ≈24 mrad, and the inner and outer angles of the detector were 90 and 370 mrad, respectively. The average size of the Pd species was analyzed based on the statistics of over 100 clusters. To analyze the decomposition temperature of $(NH_4)_2[Pd(NO_2)_2(C_2O_4)]\cdot nH_2O$, TGA measurements were performed using a NETZSCH STA 409 analyzer. In a 25 vol.% O_2/N_2 atmosphere, 30 mg of the sample was heated at a rate of 5 °C min^{-1} from room temperature to 700 °C. The loading contents of the Pd/Al_2O_3 adsorbents were determined using ICP-AES and a Varian 715-ES instrument. The ICP samples were mineralized via fusion with sodium peroxide and dissolved in a mixture of HNO_3, HF, and $HClO_4$. The crystallinity of the prepared adsorbents was characterized via PXRD. The PXRD patterns of the adsorbents were measured using a Bragg–Brentano diffractometer (Rigaku D/Max-2000) with monochromatic Cu Kα radiation ($\lambda = 0.15418$ nm). The samples were scanned from a 2θ value of 10–90° with a 2° min^{-1} scan speed. The X-ray tube was operated at a voltage and current of 40 kV and 40 mA, respectively. The FTIR spectra of the CO adsorption measurements were obtained on an IS 50 spectrometer. Before conducting the experiments, the sample (20 mg) was reduced in situ in pure H_2 at 300 °C in a cell. Subsequently, the temperature was cooled to 30 °C by placing the reaction mixture under a He atmosphere for 60 min. Additionally, a background spectrum was recorded for the sample, which was automatically subtracted from the subsequent spectra. The corresponding gas for CO adsorption (10 vol% CO/He) was introduced into the reaction cell, and the spectrum was recorded as a function of time until saturation. He flow was then switched on to purge the gaseous CO. All the total flow rates were 20 mL min^{-1}. The XPS spectra of the catalysts were recorded on a Thermo Fisher ESCALAB 250 spectrometer with a monochromatized Al-Kα X-ray source (1486.6 eV) and an applied power of 150 W. The binding energies were calibrated using the C 1s level (284.8 eV) as the internal standard. The Pd dispersion was calculated from the CO chemisorption data. CO chemisorption experiments were performed on a CHEMBET 3000 automated chemisorption instrument equipped with a thermal conductivity detector using volumetric pulse techniques in He as the carrier gas at 100 mL min^{-1}. The catalyst sample (≈100 mg) was placed in a quartz U-tube reactor. Subsequently, the catalyst was cleaned by heating in flowing He at 350 °C for 30 min, cooled to ≈30 °C in He, and pulsed ten times with CO at 30 °C. The number of exposed surfaces Pd atoms Ns was calculated by assuming that CO is adsorbed stoichiometrically on the surface Pd atoms. The actual Pd loading determined the total number of Pd atoms in the catalyst (Nt). Pd dispersion (R) was calculated using Equation (3), as follows:

$$R = \frac{N_s}{N_t} \times 100\% \tag{3}$$

Supporting Information

Supporting Information is available from the Wiley Online Library or from the author.

Acknowledgements

Conflict of Interest

The authors declare no conflict of interest.

Data Availability Statement

The data supporting the findings of this study are available from the corresponding author upon reasonable request.

[1] Y. Xie, J. Bao, X. Song, X. Sun, P. Ning, C. Wang, F. Wang, Y. Ma, M. Fan, L. Kai, *J. Hazard. Mater.* **2023**, *442*, 130029.
[2] X. Zhang, Y. Zhou, G. Li, Z. Lei, C. Yin, Y. Yang, H. Wang, F. Feng, L. Wei, Q. Zhang, F. Yang, L. Lin, C. Lu, X. Li, *Appl Catal B* **2022**, *315*, 121566.
[3] M. Zhang, J. Guan, Y. Tu, S. Chen, Y. Wang, S. Wang, L. Yu, C. Ma, D. Deng, X. Bao, *Environ Sci* **2020**, *13*, 119.
[4] Y. Huang, D. Ma, W. Liu, D. Xia, L. Hu, J. Yang, P. Liao, C. He, *Environ. Sci. Technol.* **2021**, *55*, 16723.
[5] J. Huang, S. Zhong, Y. Dai, C. Liu, H. Zhang, *Environ. Sci. Technol.* **2018**, *52*, 11309.
[6] J. Lu, H. Hao, L. Zhang, Z. Xu, L. Zhong, Y. Zhao, D. He, J. Liu, D. Chen, H. Pu, S. He, Y. Luo, *Appl Catal B* **2018**, *237*, 185.
[7] H. Wang, Z. Huang, Z. Jiang, Y. Zhang, Z. Zhang, S. Wang, *ACS Catal.* **2018**, *8*, 3164.
[8] N. An, H. Wang, M. Zhang, J. Xie, Y. Dai, X. Yuan, L. Geng, *Chemosphere* **2020**, *256*, 127077.
[9] J. Guo, M. Janik, C. Song, *J. Phys. Chem. C* **2012**, *116*, 3457.
[10] J. Xie, H. Jiang, S. Guo, *ACS Appl. Nano Mater.* **2021**, *4*, 3044.
[11] L. Uros, V. Rastko, T. Tomasz, C. Grzegorz, Z. Piotr, E. Nevenka, K. Nedeljko, *Nano Energy* **2018**, *47*, 527.
[12] B. Wang, Y. Yue, C. Jin, J. Lu, S. Wang, L. Yu, L. Guo, R. Li, Z. Z. Hu, J. Zhao, X. Li, *Appl Catal B* **2020**, *272*, 118944.
[13] Y. Liu, A. McCue, C. Miao, J. Feng, D. Li, J. Anderson, *J. Catal.* **2018**, *364*, 406.
[14] B. Xu, Y. Zhang, L. Li, Q. Shao, X. Huang, *Coordin. Chem. Rev.* **2022**, *459*, 214388.
[15] J. Kim, Y. Jo, J. Kim, M. Cho, S. Lee, H. Choi, *Chemosphere* **2022**, *307*, 135838.
[16] E. Jardim, S. Frances, F. Coloma, J. Anderson, J. Silvestre, *J. Colloid Interface Sci.* **2015**, *443*, 45.
[17] M. Konishcheva, D. Potemkin, P. Snytnikov, O. Stonkus, V. Belyaev, V. Sobyanin, *Appl Catal B* **2018**, *221*, 413.
[18] X. Zhu, B. Cheng, J. Yu, W. Ho, *Appl. Surf. Sci.* **2016**, *364*, 808.
[19] P. Destro, S. Marras, L. Manna, M. Colombo, D. Zanchet, *Catal. Today* **2017**, *282*, 105.
[20] Y. Zhao, W. Liang, Y. Li, L. Lefferts, *Catal. Today* **2017**, *297*, 308.

**ADVANCED
SCIENCE NEWS**

www.advancedsciencenews.com

**ADVANCED
FUNCTIONAL
MATERIALS**

www.afm-journal.de

[21] D. Gao, S. Wang, C. Zhang, Z. Yuan, S. Wang, *Chin. J. Catal.* **2008**, *29*, 1221.

[22] F. Gracia, J. Miller, A. Kropf, E. Wolf, *J. Catal.* **2002**, *209*, 341.

[23] D. Zhang, D. Yang, S. Wang, L. Zeng, J. Xin, H. Zhang, A. Lei, *Chin. J. Chem.* **2021**, *39*, 307.

[24] M. Emmert, A. Cook, Y. Xie, S. Sanford, *Angew. Chem., Int. Ed.* **2011**, *50*, 9409.

[25] W. Liu, Q. Ye, J. Jiang, L. Lou, Y. Xu, C. Xie, M. Xie, *ChemMedChem* **2013**, *8*, 1465.

[26] X. Chen, Q. Ye, M. Xie, J. Chen, Z. Pan, W. Liu, *Res. Chem. Intermed.* **2012**, *38*, 421.

[27] P. Tan, Y. Jiang, L. Sun, X. Liu, K. AlBahily, U. Ravon, A. Vinu, *J. Mater. Chem. A* **2018**, *6*, 23978.

[28] A. Maldonado, R. Yang, *J. Am. Chem. Soc.* **2004**, *126*, 992.

[29] M. Roger, O. Krocher, D. Ferri, *Chem. Eng. J.* **2023**, *451*, 138865.

[30] J. Fu, J. Dong, R. Si, K. Sun, J. Zhang, M. Li, N. Yu, B. Zhang, M. Humphrey, Q. Fu, *ACS Catal.* **2021**, *11*, 1952.

[31] Y. Lou, Y. Cai, W. Hu, L. Wang, Q. Dai, W. Zhan, Y. Guo, P. Hu, X. Cao, J. Liu, *ACS Catal.* **2020**, *10*, 6094.

[32] M. Zhu, X. Du, Y. Zhao, B. Mei, Q. Zhang, F. Sun, Z. Jiang, Y. Liu, H. He, Y. Cao, *ACS Catal.* **2019**, *9*, 6212.

[33] C. Wang, Y. Li, C. Zhang, X. Chen, C. Liu, W. Weng, W. Shan, H. He, *Appl Catal B* **2021**, *282*, 119540.

[34] L. Zhou, S. He, Y. Sang, X. Zhang, H. Liu, C. Jia, X. Xu, *Catal. Commun.* **2020**, *142*, 106034.

[35] X. Gao, W. Lu, S. Hu, W. Li, A. Lu, *Chin. J. Catal.* **2019**, *40*, 184.

[36] D. Liu, P. Bai, P. Wu, D. Han, Y. Chai, Z. Yan, *Appl. Surf. Sci.* **2015**, *351*, 250.

[37] K. Cychosz, A. Foy, A. Matzger, *J. Am. Chem. Soc.* **2009**, *131*, 14538.